Effect of near-bed turbulence on chronic detachment of epilithic biofilm: Experimental and modeling approaches.

Myriam Graba, Frédéric Moulin, Stéphanie Boulêtreau, Frédéric Garabétian, Ahmed Kettab, Olivier Eiff, José Miguel Sanchez-Pérez, Sabine Simeoni-Sauvage

Effect of near-bed turbulence on chronic detachment of epilithic biofilm: Experimental and modeling approaches

Myriam Graba,[1,2] Frédéric Y. Moulin,[3] Stéphanie Boulêtreau,[1] Frédéric Garabétian,[4] Ahmed Kettab,[2] Olivier Eiff,[3] José Miguel Sánchez-Pérez,[1] and Sabine Sauvage[1]

Received 24 September 2009; revised 23 June 2010; accepted 6 July 2010; published 20 November 2010.

[1] The biomass dynamics of epilithic biofilm, a collective term for a complex microorganism community that grows on gravel bed rivers, was investigated by coupling experimental and numerical approaches focusing on epilithic biofilm-flow interactions. The experiment was conducted during 65 days in an artificial rough open-channel flow, where filtered river water circulated at a constant discharge. To characterize the effect of near-bed turbulence on the chronic detachment process in the dynamics of epilithic biofilm, local hydrodynamic conditions were measured by laser Doppler anemometry and turbulent boundary layer parameters inferred from double-averaged quantities. Numerical simulations of the EB biomass dynamics were performed using three different models of chronic detachment based upon three different descriptors for the flow conditions: Discharge Q, friction velocity u_*, and roughness Reynolds number k^+. Comparisons of numerical simulation results with experimental data revealed chronic detachment to be better simulated by taking the roughness Reynolds number as the external physical variable forcing chronic detachment. Indeed, the loss of epilithic matter through the chronic detachment process is related not only to hydrodynamic conditions, but also to change in bottom roughness. This suggests that changes in the behavior and dimensions of river bed roughness must be considered when checking the dynamics of epilithic biofilm in running waters.

Citation: Graba, M., F. Y. Moulin, S. Boulêtreau, F. Garabétian, A. Kettab, O. Eiff, J. M. Sánchez-Pérez, and S. Sauvage (2010), Effect of near-bed turbulence on chronic detachment of epilithic biofilm: Experimental and modeling approaches, *Water Resour. Res.*, *46*, W11531, doi:10.1029/2009WR008679.

1. Introduction

[2] "Epilithic biofilm" is a collective term for a complex microorganism community that grows on gravel, cobbles, and rocks in river beds and includes algae, bacteria, and microfauna, with algae usually the dominant component. This community plays a major role in fluvial ecosystems because it is the source of most primary production [*Minshall*, 1978; *Lock et al.*, 1984], and constitutes a food source for a number of invertebrates and fish [*Fuller et al.*, 1986; *Mayer and Likens*, 1987; *Winterbourn*, 1990]. It also plays a major role in the metabolic conversion and partial removal of biodegradable material in rivers and streams [*McIntire*, 1973; *Saravia et al.*, 1998; *Hondzo and Wang*, 2002]. Thus, for better management of fluvial ecosystems dominated by fixed biomass in the near-bed region, epilithic biofilm dynamics should be considered in numerical modeling of biogeochemical transfer.

[3] A large number of models have been designed to describe the biomass dynamics of the epilithic biofilm. Some complex models focus on different component species of the epilithic biofilm [e.g., *Asaeda and Hong Son*, 2000, 2001; *Flipo et al.*, 2004], whereas simpler models [e.g., *McIntire*, 1973; *Horner and Welch*, 1981; *Horner et al.*, 1983; *Momo*, 1995; *Uehlinger et al.*, 1996; *Saravia et al.*, 1998] relate the peak biomass of epilithic biofilm to environmental variables such as nutrient concentration, light intensity, and flow discharge. The main processes involved in these models can be summarized in $dB/dt = C + G - D$, where B is the biomass, C the colonization function, G the growth function, and D the detachment function, which can describe chronic, autogenic, or catastrophic detachment, or a combination of these. These models have been developed either to explain processes observed in natural streams and rivers [*Uehlinger et al.*, 1996; *Saravia et al.*, 1998] or in artificial channels and laboratory streams [*McIntire*, 1973]. In some cases, the processes of colonization and growth are not modeled separately [*Horner and Welch*, 1981; *Horner et al.*, 1983] or the detachment process is ignored [*Momo*, 1995].

[4] Among these models, that of *Uehlinger et al.* [1996] has been most frequently used for natural or artificial river flows [*Fothi*, 2003; *Boulêtreau et al.*, 2006, 2008; *Labiod et al.*, 2007]. In fact, although this model has been applied

[1]ECOLAB, Université de Toulouse, UPS, INPT, CNRS, Toulouse, France.
[2]Laboratoire des Sciences de l'Eau, Ecole Nationale Polytechnique, Algiers, Algeria.
[3]IMFT, Université de Toulouse, UPS, INPT, ENSEEIHT, CNRS, Toulouse, France.
[4]UMR 5805, Station Marine d'Arcachon, EPOC-OASU, Université Bordeaux 1, Arcachon, France.

0043-1397/10/2009WR008679

successfully to reproduce the temporal variations in epilithic biofilm biomass in natural rivers (Swiss pre-alpine gravel bed river systems) [*Uehlinger et al.*, 1996], it had been developed earlier by *McIntire* [1973] through experiments in laboratory open-channel flows. This model was recently applied by *Boulêtreau et al.* [2006] to the large Garonne River using an additional term to include autogenic detachment. The level of complexity of this model was also investigated by using the Akaike Information Criterion (AIC) to determine the minimum adequate parameter set required to describe the biomass dynamics. *Boulêtreau et al.* [2006] found that in 9 of the 11 cases studied, the best model was one that described an equilibrium between phototrophic growth and discharge-dependent chronic loss, and that ignored light, temperature, nutrient influences, and catastrophic and/or autogenic detachment terms. This simplified model is

$$\frac{dB}{dt} = G - D = \underbrace{\mu_{max} B}_{G1} \underbrace{\frac{1}{1 + k_{inv} B}}_{G2} - \underbrace{C_{det} Q\, B}_{D}, \qquad (1)$$

where B (g m^{-2}) is the epilithic biofilm biomass, t (days) is the time, μ_{max} (d^{-1}) is the maximum specific growth rate at the reference temperature 20°C, k_{inv} (g^{-1} m^2) is the inverse half-saturation constant for biomass, C_{det} (s m^{-3} d^{-1}) is an empirical detachment coefficient, and Q (m^3 s^{-1}) is the flow discharge. In this simplified model, G is a growth function formed by the linear term $G1$, which describes the exponential increase in biomass, and the term $G2$, which describes the effect of density limitation and characterizes the biomass limitation of the growth rate. It accounts for the phenomenon of biomass growth rate decreasing with increasing epilithic biofilm mat thickness, due to limitations in light and nutrient concentration in the inner layers of the biofilm. Term D is the detachment function, which is controlled here by Q and B, and does not take into account grazing or catastrophic loss of biomass due to bed movement. These two latter processes were assumed negligible or nonexistent in our laboratory experiments.

[5] Several previous studies have investigated the mutual influences of epilithic biofilm and stream flow. Early studies focusing on the effect of current on epilithic biofilm accrual showed that there is intraspecific competition in the epilithic biofilm assemblage, mainly driven by current velocity [*Ghosh and Gaur*, 1998]. Some authors [e.g., *Horner and Welch*, 1981; *Stevenson*, 1983] observed a positive correlation, with biomass increasing in proportion to increasing velocity, whereas others [*Ghosh and Gaur*, 1998] found an inverse relationship between epilithic accumulation and current velocity.

[6] At present, it is generally recognized that flow is an important factor involved directly or indirectly in many relevant processes (e.g., colonization, metabolism, nutrient fluxes, and detachment) of epilithic biofilm dynamics [*Stevenson*, 1983; *Reiter*, 1986; *Uehlinger et al.*, 1996; *Saravia et al.*, 1998; *Hondzo and Wang*, 2002; *Boulêtreau et al.*, 2006, 2008]. Retroactively, its presence and its age are important factors that modify local hydrodynamic characteristics such as the equivalent roughness height k_s and the friction velocity u_*. *Reiter* [1989a, 1989b] and *Nikora et al.* [1997, 1998] found that u_*, which measures the drag of the flow at the bottom, increased with the growth of the epilithic biofilm, leading to the conclusion that epilithic biofilm increased bed roughness. In contrast, *Biggs and Hickey* [1994] observed that epilithic biofilm decreased the roughness of the substratum.

[7] These early studies demonstrated the complexity of flow-epilithic biofilm interactions and have motivated further research in the past decade [*Godillot et al.*, 2001; *Nikora et al.*, 2002; *Hondzo and Wang*, 2002; *Fothi*, 2003; *Labiod et al.*, 2007; *Moulin et al.*, 2008a]. The latter studies show that the presence of the epilithic biofilm induces a clear variation in turbulence intensity and Reynolds stress in the benthic zone. *Moulin et al.* [2008a] showed how different hydrodynamic conditions promote different growth patterns of epilithic biofilm (dense mat or porous mat with long filaments) and yield different values of the equivalent roughness height k_s, even for approximately the same amount of biomass.

[8] The interfacial region between the epilithic biofilm and the flow plays a major role, and its description requires local parameters associated with the turbulent processes instead of vertically integrated quantities such as flow discharge or mean longitudinal velocity (as used in the detachment term by *Horner and Welch* [1981], *Horner et al.* [1983], and *Saravia et al.* [1998]). Thus, *Fothi* [2003] suggested replacing the flow discharge Q with the roughness Reynolds number $k^+ = u_* k_s/\nu$ (where ν is water kinetic viscosity and k_s the equivalent roughness height) in the detachment term of the model by *Uehlinger et al.* [1996]. However, *Labiod et al.* [2007] adopted an intermediate step by taking the friction velocity u_* as an external physical parameter for the detachment. First evaluations of these models [*Fothi*, 2003; *Labiod et al.*, 2007] with laboratory experiments in open-channel flows gave better results than the early model of *Uehlinger et al.* [1996]. However, additional experimental data are required to determine the relevance of $u*$ or k^+ alone to describe the chronic detachment term. The main objective of the present study was to test and compare these two equations of the chronic detachment term through further experiments and to help answer the central question that stream biologists ask their physics colleagues [see *Hart and Finelli*, 1999], i.e., "What flow parameters should be measured to obtain the most appropriate quantification of the physical environment for stream biota?" when discussing the epilithic biofilm chronic detachment process.

2. Theoretical Background

2.1. Spatial Averaged Flow and Log Law Formulation

[9] It should be noted that our experiment was conducted in steady, uniform, open channel flow, over a rough bed with a high relative submergence (flow depth $H \gg$ roughness height Δ). In such free surface turbulent boundary layers, it is possible to distinguish three principal layers [see, e.g., *Nikora et al.*, 2001, 2007a, 2007b]: (1) An outer layer ($z > 0.2\ H$), (2) a logarithmic layer that occupies the flow region (2–5) $\Delta < z < 0.2\ H$, and (3) a roughness layer composed of a form-induced sublayer in the region just above the roughness crests $\Delta < z <$ (2–5) Δ and an interfacial sublayer (or canopy) that occupies the flow region below the crests $z < \Delta$.

[10] Recently, *Lopez and Garcia* [1998, 2001] and *Nikora et al.* [2002] demonstrated experimentally and theoretically that in such flows over a rough bottom, double-averaged quantities (i.e., quantities averaged in time and in the two

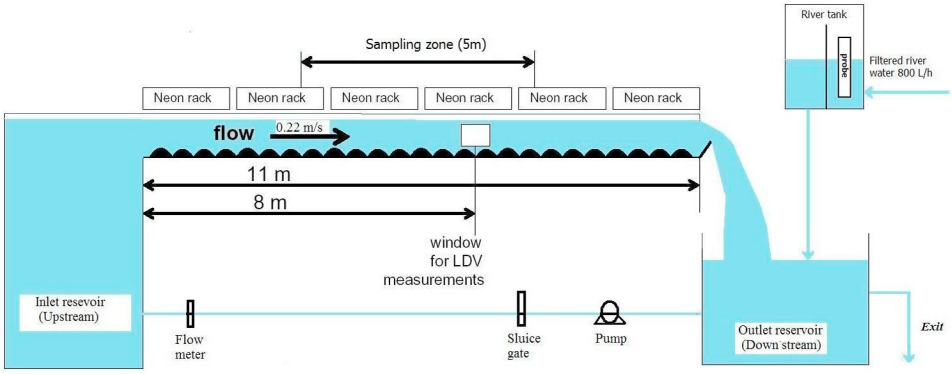

Figure 1. Longitudinal view of the experimental flume.

horizontal directions x and y and denoted $\langle\rangle_{xy}$) lead to a better description of the roughness sublayer. Double-averaging yields, for instance a quasi-linear velocity profile deep inside the roughness sublayer in the interfacial sublayer, extends the validity range of the log law towards the top of the roughness in the form-induced sublayer; thus, leading to more robust estimations of the boundary layer parameters u_*, z_0, and d [*McLean and Nikora*, 2006; *Nikora et al.*, 2007a, 2007b; *Moulin et al.*, 2008a], which appear in the generalized log law formula

$$\frac{\langle \overline{U} \rangle_{xy}}{u_*} = \frac{1}{\kappa} \ln\left(\frac{z-d}{k_s}\right) + A = \frac{1}{\kappa} \ln\left(\frac{z-d}{z_0}\right), \tag{2}$$

where κ is the Von Karman constant ($\kappa \approx 0.4$), u_* the friction velocity, z the distance from the flume bed, d the displacement length (also known as a zero-plane displacement) and $z_0 = k_s \exp(-\kappa A)$ the roughness length, and A being a constant that depends on flow regime (A ≈ 8.5 for fully rough flows, i.e., k+ > 70 [see, e.g., *Nezu and Nakagawa*, 1993]).

2.2. Chronic Detachment Function Formulation

[11] As underlined previously, the detachment equation with a global hydrodynamic parameter Q ($m^3\ s^{-1}$) [*Uehlinger et al.*, 1996] cannot realistically describe a phenomenon such as the detachment that occurs on the bed where epilithic biofilm grows. However, the function of detachment can be described in a more pertinent equation by taking as external physical variables local hydrodynamic characteristics, such as friction velocity u_* [*Labiod et al.*, 2007] or the roughness Reynolds number k^+ ($k^+ = u_* k_s/\nu$) [*Fothi*, 2003].

[12] Thus, three models can be inferred from equation (1), with three formulations for the chronic detachment function D as

$$D = d_1 = C_{\mathrm{det}} Q\, B, \tag{3}$$

$$D = d_2 = C'_{\mathrm{det}} u_* B, \tag{4}$$

$$D = d_3 = C''_{\mathrm{det}} k^+ B, \tag{5}$$

where Q ($m^3\ s^{-1}$) is the discharge flow, u_* ($m\ s^{-1}$) the friction velocity, ($k^+ = u_* k_s/\nu$) the dimensionless roughness Reynolds number, and C_{det} ($s\ m^{-3}\ d^{-1}$), C'_{det} ($s\ m^{-1}\ d^{-1}$), and C''_{det} (d^{-1}) the detachment coefficients.

3. Materials and Methods

3.1. Experimental Design and Procedure

[13] The experiment was performed in the indoor experimental flume used by *Godillot et al.* [2001] and *Labiod et al.* [2007], located at the Institute of Fluid Mechanics, Toulouse, France. The flume is 11 m long, 50 cm wide, and 20 cm deep, with Plexiglas sides (10 mm thick) and a PVC base (20 mm thick). The bed slope is 10^{-3} and the hydraulic circuit is a closed loop. For the present study, this experimental flume was modified to run using a partial recirculation system, thereby allowing the use of Garonne River water with no nutrient limitation, but with complete control of the hydrodynamic conditions. The partial recirculation system (Figure 1) consists of an initial pump (Selfinox 200/80T, ITT Flygt) that continuously supplies water from the river to the outlet reservoir (3300 L) with a flow discharge of 800 L h^{-1} (ensuring a complete turnover of water in the system every 4 h), and a second submerged pump (Omega 10-160-4, Smedegard) that supplies water to the inlet reservoir (1500 L). The water flows by gravity through the experimental flume from the inlet reservoir to the outlet reservoir. Convergent and guiding grids are placed in the inlet reservoir to ensure quasi-uniform entry flow. A moderate current velocity (0.22 m s^{-1}) was selected in the present study to enhance microorganism colonization and growth [*Stevenson*, 1983].

[14] The Garonne River water was treated to reduce the supply of suspended matter and to exclude grazers; large particles were eliminated by two centrifugal separators, and the water was then filtered 3 times through filters with 90, 20, and 10 μm pores. Light was supplied by six 1.5 m long racks of five evenly distributed neon tubes ("daylight", Philips TLD 58 W) and fluorescent tubes (Sylvania Gro-Lux 58 W; designed for enhancing photosynthesis as they emit in the visible red area). Photoperiod was set at 16 hours of day and 8 hours of night. The incident light, measured with an LI-190SA quantum sensor and an LI-1000 data logger (LI-COR), varied between 140 and 180 μmol $m^{-2}\ s^{-1}$ photosynthetically active radiation (PAR) on the channel bottom, ensuring photosynthetic activity saturation [*Bothwell et al.*, 1993].

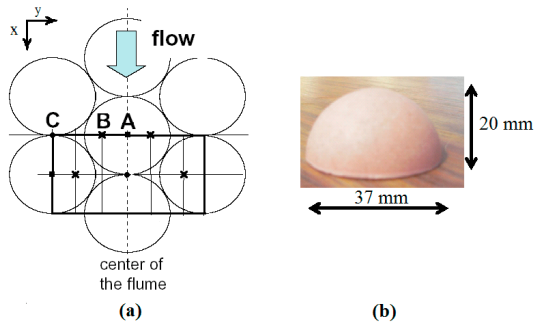

Figure 2. (a) Positions of the vertical profiles A, B, and C for LDA measurements and double-averaging ($<Values>_{xy}$ = (2 Values in A + 4 Values in B + 2 Values in C)/8 = (Values in A + 2 Values in B + Values in C)/4). (b) Photograph of an artificial cobble.

[15] The bottom of the flume is completely covered by artificial cobbles that mimic natural cobbles (see Figure 2). Each artificial cobble consists of a chemically inert sand-ballasted polyurethane resin hemisphere (37 mm diameter, 20 mm high), with a shape and texture shown to provide good conditions for epilithic biofilm adhesion and growth [*Nielsen et al.*, 1984] and with a resistance to temperature of 110°C. To eliminate any possible toxicity due to artificial cobble manufacture (e.g., solvents), cobbles were immersed in river water for 3 weeks, then washed with tap water and sterilized by autoclave (120°C, 20 min) before being positioned side by side in the flume. The artificial cobbles are not fixed in place so that they could be sampled.

[16] To obtain diverse epilithic biofilm communities, pebbles (average size 10 cm^2) with biofilm were collected in southwest France streams (Ariège (09) and Gave de Pau (05)) and rivers (Garonne (7) and Tarn (8)) displaying a wide range of hydroecological conditions. These pebbles were stored in another running flume that was dedicated to providing biofilm matter for our experiment. A biofilm suspension was produced by scraping the upper surface of 15 randomly selected pebbles with a toothbrush, and adding the obtained product to 1 L of filtered (0.22 μm pore size) water. The biofilm suspension was crushed, then homogenized (tissue homogenizer) to remove macrofauna and approach a grazer-free condition. For 3 weeks, the flume was run using closed recirculation; that is, the water was renewed weekly, and just after renewal, it was seeded with the prepared biofilm suspension. After the seeding (inoculum) stage, the closed circulation flume was changed to an open circulation flume to allow free growth of epilithic biofilm on the bed in water without nutrient limitation. During the epilithic biofilm growth experiment (65 days), which comprised several stages, hydrodynamic and biological measurements were performed and upper view photographs of the artificial cobbles were taken daily through a Plexiglas window located at the water surface (Nikon camera with 194 2000 × 1312 pixel resolution).

3.2. Biological Sampling and Measurements

3.2.1. Epilithic and Drift Biomass

[17] After the seeding phase, biofilm biomass was sampled every week randomly along a 5 m length in the center of the experimental flume (see Figure 1). The three rows of cobbles closest to the walls of the flume were not sampled to avoid edge effects. To minimize the errors of measurement without disrupting the experiment, 10 cobbles were extracted on each sampling occasion and kept in sterile vials at 4°C. Subsequently, six were used to measure Ash Free Dry Mass (AFDM) and four to measure chlorophyll-*a* (Chl-*a*) mass by developed surface. Every cobble sampled was replaced with a new pink-colored one, to avoid resampling. Cobbles used for AFDM determination were dried (80°C, overnight), weighed (W_1), and scraped. Cobbles were then cleaned and weighed (W_2) to obtain Dry Mass (*DM*) by difference between W_1 and W_2. One portion (around 25 mg) of scraped dry matter was weighed before and after combustion (500°C, overnight) to determine AFDM.

[18] For Chl-*a* mass determination, biofilm was scraped from the upper surface of the four other cobbles with a sterile toothbrush, and suspended in filtered (0.2 μm, Whatman cellulose nitrate membrane) water (50 or 100 mL according to biomass). Suspensions were homogenized (tissue homogenizer) and a 10 mL aliquot was centrifuged (12000 × *g*, 20 min, 4°C). After removing the supernatant, the pellet was stored at −80°C, and Chl-*a* was measured spectrophotometrically using trichromatic equations [*Jeffrey et al.*, 1997] after extraction with 90% acetone (4 hours, darkness, room temperature) of the suspended (tissue homogenizer) and ground (ultrasonic disintegrator) pellets.

3.2.2. Algal Composition

[19] Biofilm was removed from the upper surface of one cobble with a sterile toothbrush and suspended in filtered (0.2 μm) water (50 mL) for algal composition. The biofilm suspension was preserved with glutaraldehyde (1% final concentration) and stored refrigerated in darkness until examination at 600 to 1000 X. Taxa were identified to the lowest practical taxonomic level; usually to species, but often to genus. For practical reasons, five of seven samples were selected for analysis to observe changes in taxonomic composition.

3.3. Hydrodynamic Measurements

[20] Water discharge was controlled by a sluice gate and a bypass, and measured by an electromagnetic flow meter placed in the return pipe of the flume. The water depth was measured with a millimeter scale.

[21] To estimate double-averaged quantities with a Laser Doppler Anemometer (LDA), the velocity components were measured at the centerline of the flume and in a section equipped with glass windows located 8 m from the flume entrance (Figure 1). The measurement points were situated at heights varying from 20 to 120 mm from the bottom (with 2 mm space intervals between z = 20 and 50 mm, and 10 mm intervals up to z =120 mm) along three contrasting vertical profiles A, B, and C (Figure 2). The bottom (z = 0) corresponds to the level of the bed flume without hemispheres. A Spectra-Physics bi-composant Argon Laser equipped with a 55L modular optic Disa and with wavelengths of 514.5 nm (green ray) and 488 nm (blue ray) was used. This device was placed on a support that was fixed in the longitudinal direction but that allowed horizontal and vertical movement. Signal acquisition was obtained with a photomultiplicator placed in the broadcast lamp and recovered by a Burst Spectrum Analyzer (BSA), which processed the Doppler

signal and calculated the Doppler frequency and then the instantaneous velocities. The data obtained were then processed and stored in a computer with Dantec Burstware 2.00 software.

[22] For each measurement point, data acquisition was performed during 4 minutes of n LDA observations ($n = 10^4$ to 1.5×10^4) with instantaneous longitudinal U, transverse V, and vertical W velocity components, from which time-averaged velocity components $\overline{U}$, $\overline{V}$, root-mean-square (RMS) values of the turbulent fluctuations u', v', and w', and the mean turbulent shear stress $\overline{u'w'}$ were inferred. Observations of $n = 10^4$ yielded good estimation of the averaged velocities, but $n = 1.5 \times 10^4$ acquisitions were necessary for convergence of the mean turbulent shear stress. The double-averaged turbulent shear stress $\langle\overline{u'w'}\rangle_{xy}$ and longitudinal velocity $\langle\overline{U}\rangle_{xy}$ profiles were obtained by space-averaging with respective weight factors of 1, 2, and 1 for the measurements in the three vertical profiles A, B, and C, respectively (see Figure 2), in accordance with the influential area of the three profiles. At the beginning of the experiment, measurements of the vertical velocity W were not available because of a malfunction of the W laser beam.

[23] To infer the friction velocity u_* from the turbulent quantities, we followed *Cheng and Castro* [2002] when the double-averaged turbulent shear stress $\langle\overline{u'w'}\rangle_{xy}$ was available, using

$$u_* = \lim_{z \to d} \sqrt{\langle\overline{u'w'}\rangle^2_{xy}}. \tag{6}$$

When the double-averaged turbulent shear stress was not available, we followed *Labiod et al.* [2007] and used the values of the space averaged $u_{\mathrm{rms}} = \sqrt{\overline{u'^2}}$ to fit in the exponential profiles of *Nezu and Nakagawa* [1993]:

$$\frac{\sqrt{\overline{u'^2}}}{u_*} = D_u \exp\left(-C_k \frac{z}{H-d}\right), \tag{7}$$

where C_k and D_u are empirical constants ($C_k = 1$ and $D_u = 2.3$).

[24] The double-averaged velocity profiles $\langle\overline{U}\rangle_{xy}$ were then fitted with the log law to determine z_0 and d by choosing the best values inferred from a linear regression of $\exp(\kappa\ \langle\overline{U}\rangle_{xy}/u_*) = (z-d)/z_0$ in the region between the top of the cobbles at $z = \Delta$ and the top of the logarithmic layer taken as $z = 0.2\ H$ [*Wilcock*, 1996], followed by a nonlinear best fit of $\kappa\ \langle\overline{U}\rangle_{xy}/u_* = \log(z\text{-}d) - \log(z)$ (to be consistent with previous works where the log law is generally fitted in the (U, $\log(z-d)$) plane). The equivalent roughness height k_s established by Nikuradse was inferred from $k_s = z_0 \exp(\kappa\ 8.5)$, and the roughness Reynolds number k^+ from $k^+ = u_*\ k_s/\nu$ [*Nezu and Nakagawa*, 1993].

[25] In the LDA measurements, difficulties were encountered with the algal filaments, which moved and disturbed data acquisition. However, the top of the biofilm mat could then be defined as the lowest height of validated measurements, and was therefore used as the lower limit for the fitting of data with the log law.

3.4. Numerical Model Description

[26] We noted that in equation (1), inferred from the model of *Uehlinger et al.* [1996], colonization is not considered. We therefore decided to describe the colonization process by an initial condition for the biomass, adopting a numerical parameterization [*Belkhadir et al.*, 1988; *Capdeville et al.*, 1988] to determine the value of the initial epilithic biomass denoted B_{init}.

[27] According to the considerations above, and while knowing that the factors of light, temperature, nutrient availability, and grazers were controlled in our experiment, the differential equation (1) for each of the three detachment equations (3), (4), and (5) was solved numerically by coding the fourth-order Runge-Kutta method in Fortran 90. Preliminary tests demonstrated that a time step fixed at 3 hours was a good condition to reduce errors caused by numerical integration. Values of the input data discharge Q, friction velocity u_*, and roughness Reynolds number k^+ at each time step were obtained by linear interpolation of the experimental data. To calibrate the models, we started by setting the values of the maximum specific growth $\mu_{\max}$ (d^{-1}), the inverse half-saturation constant k_{inv} ($\mathrm{g}^{-1}\ \mathrm{m}^2$), and the initial biomass B_{init} in the range of values reported in the literature from field, laboratory, and modeling studies for phytoplanktonic and benthic algae [*Auer and Canale*, 1982; *Borchardt*, 1996; *Uehlinger et al.*, 1996; *Boulêtreau et al.*, 2008]. The parameters C_{det}, C'_{det}, and C''_{det} were then adjusted to best fit the simulated values of each of the three detachment equations with experimental data.

[28] Two indices were used to test the performance of the models and the agreement between measured and simulated results and to compare the efficiency of the three models tested: The χ^2 of conformity [*Uehlinger et al.*, 1996] given by

$$\chi^2 = \sum_{i=1}^{N} \left(\frac{B(t_i) - B_{\mathrm{meas},i}}{ES_{\mathrm{meas},i}}\right)^2, \tag{8}$$

and the Nash-Sutcliffe coefficient of efficiency E [*Lekfir et al.*, 2006; *Kliment et al.*, 2008] by

$$E = 1 - \frac{\sum_{i=1}^{N} \left(B_{\mathrm{meas},i} - B(t_i)\right)^2}{\sum_{i=1}^{N} \left(B_{\mathrm{meas},i} - \overline{B_{\mathrm{meas}}}\right)^2}, \tag{9}$$

where $B_{\mathrm{meas},i}$ is the measured biomass, $B(t_i)$ the predicted biomass at time i, $ES_{\mathrm{meas},i}$ is the standard error in $B_{\mathrm{meas},i}$, $\overline{B_{\mathrm{meas}}}$ is the average of all measured values, and N is the number of measurements. Generally the model is deemed perfect when E is greater than 0.75, satisfactory when E is between 0.36 and 0.75, and unsatisfactory when E is smaller than 0.36 [*Krause et al.*, 2005].

4. Results and Discussion

4.1. Biomass Dynamics Data and Algal Composition

[29] In the seeding phase, regular and homogeneous colonization patterns were observed on the artificial cobbles. The first points of colonization were located around the two front stagnation points of the flow and a curved line of epilithic matter gradually formed between these two points (Figure 3a). These observations support the idea of a strong dependence of colonization on flow structure near the cobble layer, as indicated by preliminary numerical simulations of turbulent flow by *Labiod et al.* [2007]. This young epi-

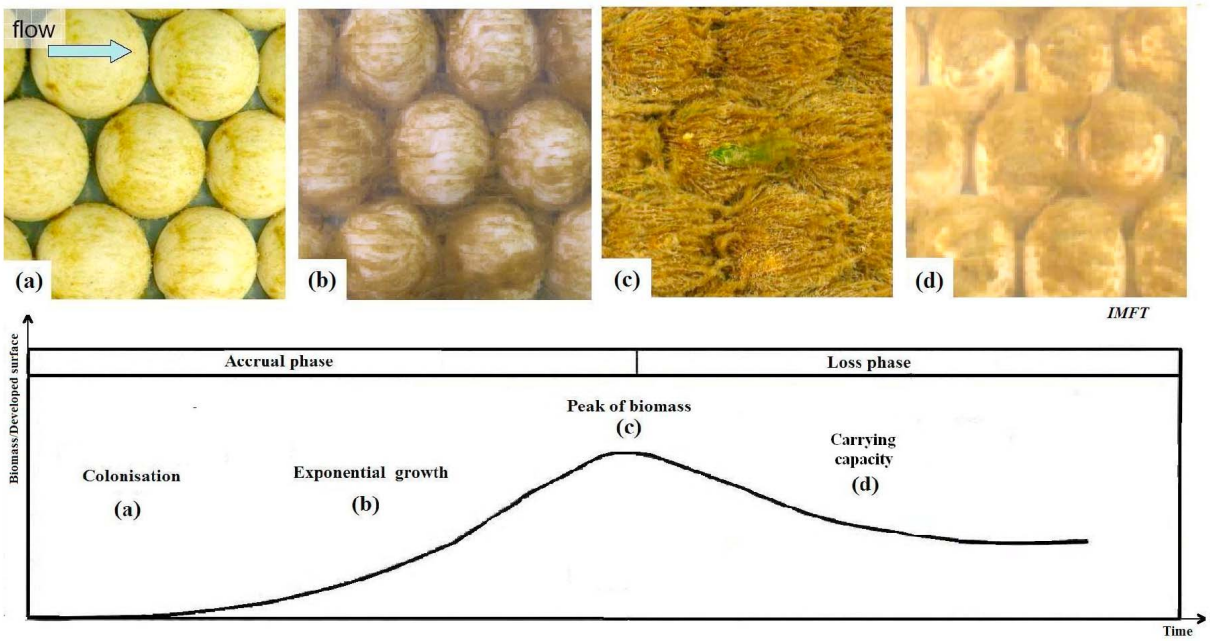

Figure 3. Biomass dynamics phases during constant discharge (14.4 $m^3 s^{-1}$) in comparison with an idealized benthic algal accrual curve [*Biggs*, 1996]: (a) 7 days after inoculum, (b) 14 days after inoculum, (c) 30 days after inoculum, (d) 52 days after inoculum.

lithic biofilm, in which the diatoms were dominant (see Table 1), then covered all surfaces exposed to the light from above, including the troughs between the cobbles. The measured values (g m^{-2}) of AFDM and Chl-*a*, with the corresponding values of the standard errors (SE, g m^{-2}) during the different stages of epilithic biofilm growth, are presented in Table 2, and are plotted in Figure 4 in terms of dimensionless numbers (c/c_{max}). In these, c is the measured AFDM or Chl-*a* and c_{max} is the maximum reached, which is equal to 32.8 ± 3.4 g m^{-2} for AFDM and 0.487 ± 0.041 g m^{-2} for Chl-*a*. Thus in the first three weeks, AFDM increased to a value of 10.5 ± 0.4 g m^{-2}, which represented 32.2 ± 1.23% of maximum growth (see Figure 4). The rate of increase then accelerated over a further 3 week period and AFDM reached 100 ± 10.5% of maximum growth at 44 days after inoculum. There followed a phase of loss, dominated by detachment, leading to a decrease to 66.1 ± 10.7% of maximum growth (21.7 ± 3.5 g m^{-2}) during the next 3 weeks. For Chl-*a*, 33.7 ± 5.85% (0.164 ± 0.028 g m^{-2}) of the maximum value was reached on day 30 after inoculum and the peak (100 ± 8.47%) was reached on day 51. The subsequent loss phase caused a decrease to 85.2 ± 10.4% of the maximum (0.415 ± 0.051 g m^{-2}) during the two last weeks.

[30] The algal community was dominated by diatoms, which represented 98–100% of the total abundance. Two taxa strongly dominated the algal community: *Fragilaria capucina* represented 46%–64% and *Encyonema minutum* represented 18%–37% of the total community, and the theoretical transition from diatoms to Chlorophyceae [*Stevenson*, 1996] was not observed, even at the end of the experiment (see Table 1).

4.2. Hydrodynamic and Boundary Layer Parameters

[31] Figure 5 shows the longitudinal velocity $\overline{U}$ at A, B, C and the double-averaged longitudinal velocity $\langle \overline{U} \rangle_{xy}$ profiles

Table 1. Relative Abundance (%) of Diatom Species at Different Biofilm Growth Stages

	Time After Inoculum (days)				
Diatom Species	23	44	51	58	65
Achnanthidium minutissimum (Kütz.) Czarnecki	0	1	0	0	2
Encyonema minutum Hilse ex. Rabenhorst	19	37	25	27	18
Encyonema silesiacum (Bleisch in Rabh.) D.G. Mann	1	3	2	0	1
Diatoma vulgaris Bory 1824	5	2	0	13	14
Fragilaria capucina Desmazieres var. *vaucheriae* (Kütz) Lange-Bertalot	64	48	55	46	57
Fragilaria crotonensis Kitton	0	0	8	12	0
Fragilaria ulna (Nitzsch.) Lange-Bert. *v. oxyrhynchus* (Kutz.) Lange-Bertalot	2	0	0	0	0
Gomphoneis minuta (Stone) Kociolek & Stoermer var. minuta	0	0	1	0	0
Comphonema parvulum (Kützing) Kützing var. *parvulum* f. parvulum	0	0	1	0	0
Gomphonema sp.	1	0	0	0	0
Fragilaria arcus (Ehrenberg) Cleve var. *arcus*	1	0	0	0	0
Melosira varians Agardh	2	1	2	1	3
Navicula tripunctata (O.F. Müller) Bory	1	1	2	0	0
Navicula sp.	1	0	0	0	0
Nitzschia acicularis (Kützing) W.M. Smith	1	0	0	0	0
Nitzschia dissipata (Kützing) Grunow var. *dissipata*	1	3	2	0	1
Nitzschia fonticola Grunow in Cleve et Möller	1	3	1	1	2
Nitzschia frustulum (Kützing) Grunow var. *frustulum*	0	0	0	0	1
Nitzschia palea (Kützing) W. Smith	0	0	0	0	1
Nitzschia sp.	0	1	0	0	0
Surirella angusta Kützing	0	0	1	0	0

Table 2. Biofilm Dynamics (Mean, ± Standard Error) Expressed as Ash-Free Dry Mass and Chlorophyll-*a*

Time After Inoculum (days)	Biomass AFDM[a] (g m^{-2})	AFDM Standard Error (g m^{-2})	Biomass Chl-*a*[b] (g m^{-2})	Chl-*a* Standard Error (g m^{-2})
23	10.5	0.4	0.079	0.005
30	18.8	1.6	0.164	0.028
37	23.3	1.3	0.230	0.039
44	32.8	3.4	0.307	0.060
51	27.0	2.8	0.487	0.041
58	23.6	3.8	0.329	0.066
65	21.7	3.5	0.415	0.051

[a]Ash-free dry mass.
[b]Chlorophyll-*a*.

produced by the LDA measurements for the bed covered with artificial cobbles before the inoculum phase (nude cobbles), and at different stages of epilithic biofilm growth. The presence and growth of the epilithic biofilm induced an acceleration of the flow and a displacement upward, associated with an adjustment of the flow in order to allow passage of the imposed discharge in the flume. Since the water depth measured from the bottom of the flume was kept constant in the present experiment, this adjustment was mainly due to a reduction in the cross-sectional area available for flow through thickening of the epilithic biofilm.

[32] The increase in longitudinal mean flow velocity is clearly perceptible in the upper part of the flow from day 16 after inoculum, but only from day 33 in the lower part (Figure 5). In fact, on day 16 after inoculum, the presence of the epilithic matter slightly reduced the depth of the flow discharge, but did not alter the shape of the roughness (see Figure 3b), which was still a more or less hemispherical pattern that led to wake drag for the flow and blocked the flow in the near-bed region. It was the increase in the thickness of the epilithic biofilm, especially in the troughs between the cobbles (see Figure 3c), that brought about a real change in the roughness topography, leading to a less rough boundary associated with less strong drag and then faster passage of the flow near the bottom. The same tendencies (acceleration and upward displacement) persisted even 61 days after inoculum, that is, during the detachment phase. This may be because the detachment occurred mainly on the lower part of the cobbles where the biofilm first began to grow and became more mature and less resistant. In addition, the detachment phase corresponded to the development on the upper part of the cobbles of long filaments, which moved and disturbed data acquisition below $z = 40$ mm (as noted at the end of section 2.3).

[33] The three turbulent shear stress profiles $\langle \overline{u'w'} \rangle_{xy}$ inferred from the LDA measurements (Figure 6) clearly exhibit linear behavior starting at zero at the free surface, as expected for open channel flow without secondary circulation [see, e.g., *Nezu and Nakagawa*, 1993], and in accordance with previous studies in the same flume [*Godillot et al.*, 2001; *Labiod et al.*, 2007] or for gravel beds [*Mignot et al.*, 2009]. The decrease in turbulent shear stress in the lower part of the profiles in Figure 6 occurred when the measurements were performed too close to the canopy layer, that is, where filaments and/or cobbles were present. Nevertheless, a decrease is always observed in the canopy layer, where the drag forces gradually counterbalance the turbulent shear stress and bring it back to values close to zero at the bottom (e.g., see *Moulin et al.* [2008b] and *Mignot et al.* [2009] for shells and gravel beds). The changes in the turbulent shear stress profiles during the experiment were very weak compared with the changes measured by *Godillot et al.* [2001] and *Labiod et al.*

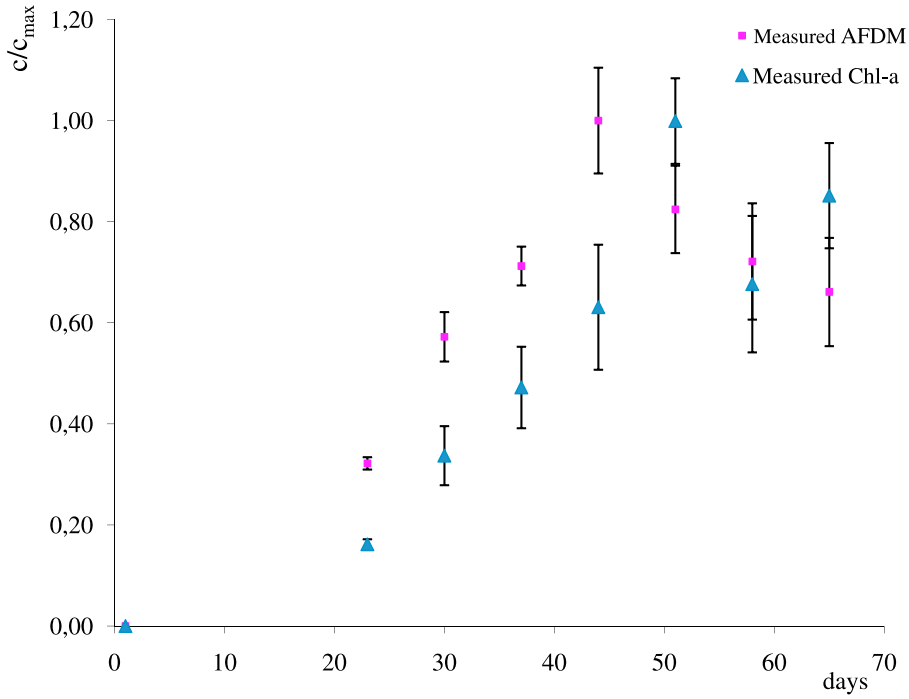

Figure 4. Evolution of the dimensionless biomass concentration (c/c_{max} ± SE) at different days after inoculum.

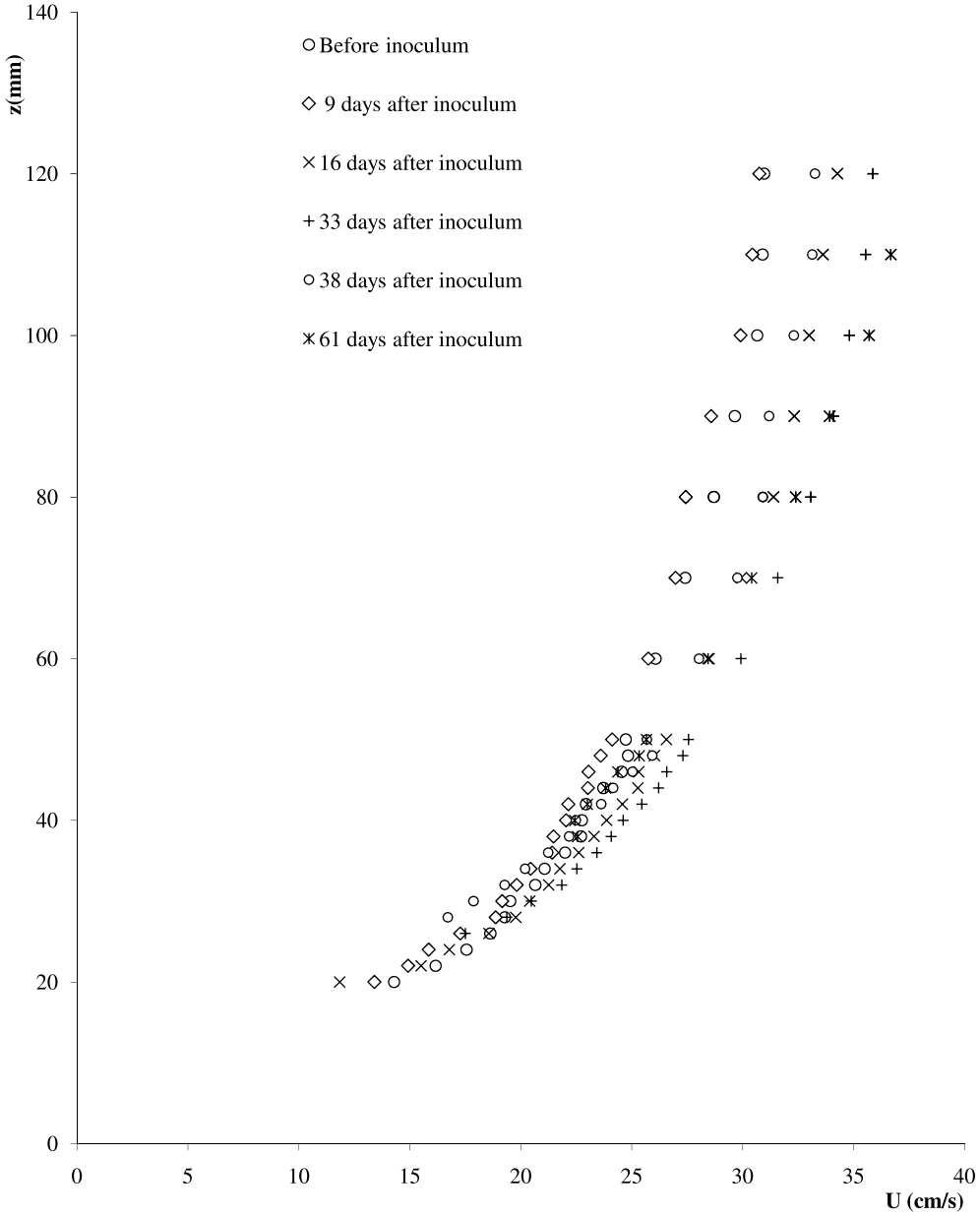

Figure 5. Double-averaged velocity profiles in the longitudinal direction obtained by LDA measurements before inoculum and 9, 16, 33, 38, and 61 days after inoculum.

[2007] in growth experiments in the same flume. However, it is worth noting that smaller substrate units were used in their experiments (rods and marbles with radii of 5 and 8 mm, respectively) for flow conditions yielding smooth, intermediate, and fully rough turbulent boundary layers in the same growth experiment. This is very different from the present experiment, where the turbulent boundary layer was fully rough from the beginning, owing to the large artificial cobbles and relatively energetic flow conditions used. In accordance with the change in $\langle \overline{u'w'} \rangle_{xy}$, the double-averaged u_{rms} ($\sqrt{\overline{u'^2}}$) profiles presented in Figure 7 remained quite similar and exhibited the exponential behavior discussed for example in *Nezu and Nakagawa* [1993] and used here to estimate the friction velocity u_* when the turbulent shear stress was not available.

[34] Values of the boundary layer parameters inferred from LDA measurements are given in Table 3. Standard error for the estimate of the friction velocity u_* was always lower than 0.0005 m s^{-1} (so is not reported in Table 3). Standard errors for the estimates of the roughness length z_0, the displacement height d and the equivalent sand roughness k_s have been calculated during the fitting procedure and reported in Table 3. In the experiments where the two different methods of obtaining u_* were available (i.e. days 33, 38 and 61), adjustments of the constants C_k and D_u in the equation (7) were investigated to obtain a match between the two methods. For the two first cases (days 33 and 38),

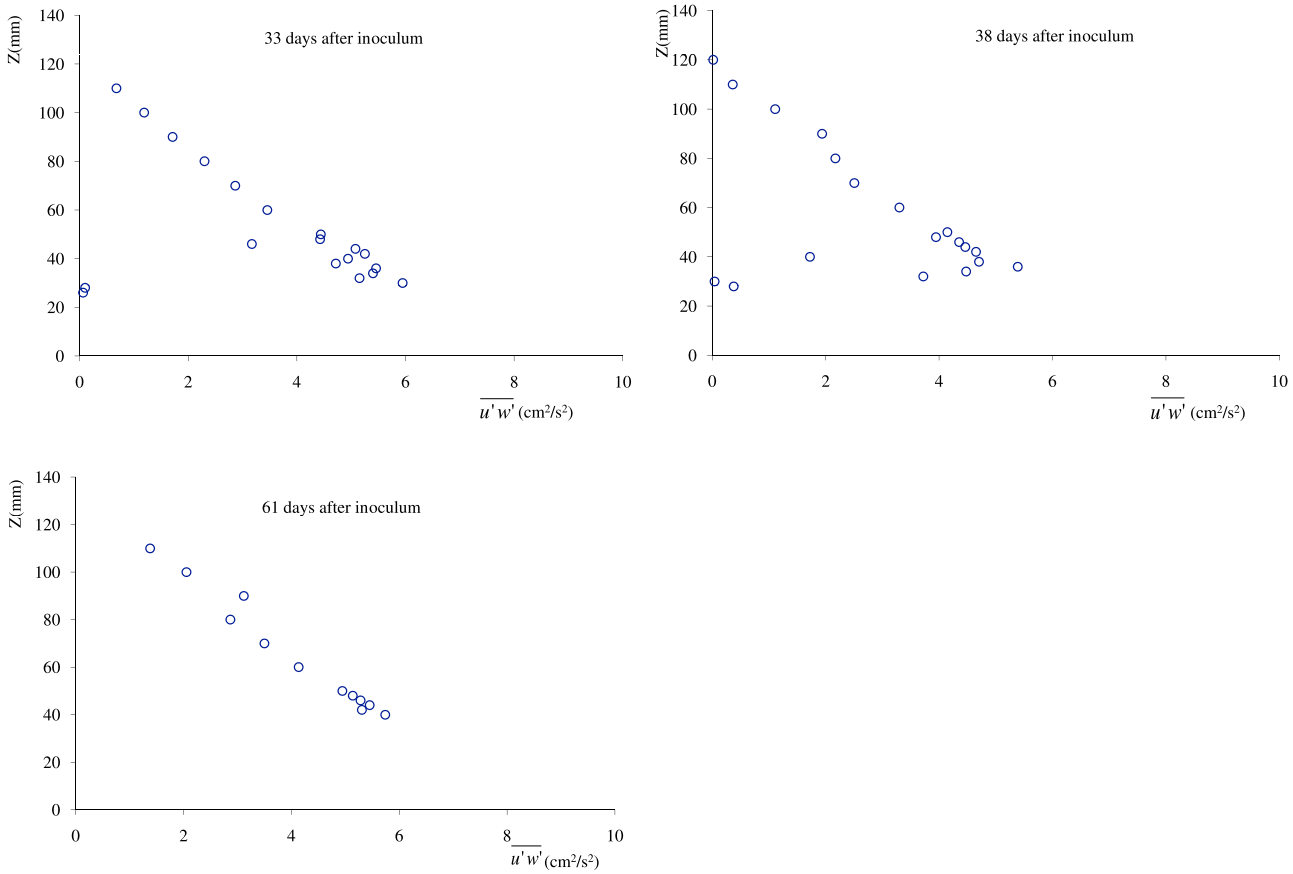

Figure 6. Double-averaged turbulent shear stress $\langle \overline{u'w'} \rangle_{xy}$ profiles in the longitudinal direction obtained by LDA measurements before inoculum and 33, 38, and 61 days after inoculum.

values of C_k remained very close to 1 and values for D_u were equal to 2.23 and 2.29, respectively, in accordance with the value of 2.3 proposed by *Nezu and Nakagawa* [1993] for solid, rough beds. Therefore, the use of the second method based upon equation (7) appears appropriate for the first stage of biofilm growth, when the biomass remained well attached to the artificial cobbles. However, the value of D_u found for day 61 decreases to 2.1, and seems to indicate a change in the nature of the turbulent flow near the bed, associated with a biofilm mat made of long filaments attached closer to the top of the artificial cobbles. The estimation of the friction velocity based upon equation (6) is then more relevant and equation (7) with a value for D_u equal to 2.3 would underestimate it.

[35] The values of the boundary parameters given in Table 3 show that the epilithic biofilm induced a decrease in the Nikuradse equivalent roughness height k_s, leading to hydraulic smoothing of the bottom. The value of the roughness length $z_0 = 0.108$ cm at the beginning of the experiment, before biofilm growth, was very close to the values of 0.115 and 0.122 cm found by *Nikora et al.* [2002] in experiments with 21 mm high and 60 mm wide caps, respectively. However, we observed a decrease in z_0 with biofilm growth, whereas *Nikora et al.* [2002] observed a 16%–21% increase when the biofilm was "well developed and growth in the periphyton biomass had saturated," something that occurred after 18 days in their experiments. Energetic flow conditions in their experiments (friction velocities u_* of 6.5 and 7.7 cm s^{-1} compared with values around 2.5 cm s^{-1} in the present study), associated with possible nutrient depletion or light limitation near the bottom, could have driven biofilm formation in a very different direction from that observed in the present study (see, e.g., *Moulin et al.* [2008b] for a discussion on the impact of flow conditions on biofilm structure). The main structural difference that can be inferred from photographs is that in their experiments, the biofilm that remained on the substrate was located near the top, as "forelocks," while in our case growth also occurred between the artificial cobbles and gradually filled the available space without any effect of nutrient depletion near the bottom. As a consequence, the forelocks at the top seemed to increase the apparent height of the roughness, leading to greater drag and increased z_0 [*Nikora et al.*, 2002], while in our case the flow, and thus the drag, were weakened by the presence of biofilm between the cobbles, leading to a decrease in z_0.

[36] Values of k_s found by *Labiod et al.* [2007] at the end of their experiments ranged between 4.7 and 11.43 mm, and our last values for the equivalent roughness height, k_s (8.4 mm at day 38 and 9.9 mm at day 61) fall inside this range. This may indicate that when the biofilm was well developed in our experiments, the surface formed by the biofilm mat was very similar to that formed in the experiments of *Labiod et al.* [2007], at least from a hydraulic point of view. In our case, the available space between the cobbles was filled, in contrast

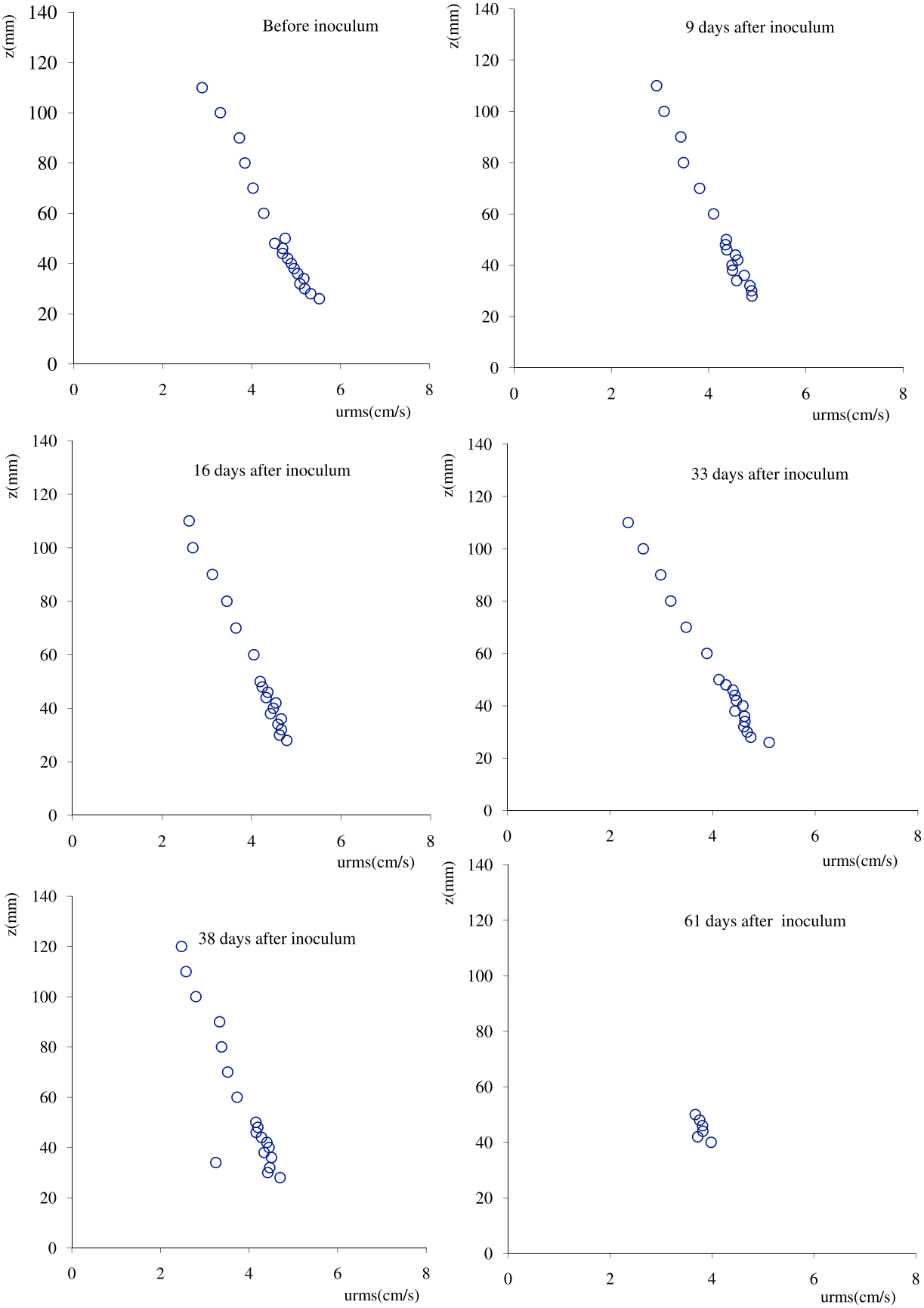

Figure 7. Double-averaged u_{rms} profiles obtained by LDA measurements before inoculum and 9, 16, 33, 38, and 61 days after inoculum.

Table 3. Discharge and Boundary Layer Parameters During Epilithic Biofilm Growth

Time After Inoculum (days)	Water Discharge Q (10^{-3} m^3 s^{-1})	Water Depth H (m)	Friction Velocity u_* (m s^{-1})	Roughness Length z_0 (cm)	Equivalent Sand Roughness ks (cm)	Displacement Height d (cm)	Roughness Reynolds Number k^+
0	14.44	0.13	0.028	0.109±0.005	3.27±0.15	1.11±0.03	915
9	14.40	0.13	0.025	0.064±0.003	1.92±0.10	1.41±0.05	480
16	14.50	0.13	0.024	0.047±0.001	1.41±0.04	1.64±0.09	338
33	14.40	0.13	0.024	0.032±0.001	0.96±0.02	1.99±0.03	230
38	14.42	0.13	0.023	0.028±0.001	0.84±0.04	2.26±0.18	193
61	14.49	0.13	0.025	0.033±0.002	0.99±0.06	2.68±0.30	247

to that in the experiments of *Nikora et al.* [2002]. This filling of the available space between the cobbles and the thickening of the biofilm mat was also very apparent from the change in d, which increased gradually from 1.11 to 2.7 cm. On the whole, the gradual decrease in k_s can be interpreted as a transition from a drag due to the same nude artificial cobbles as reported by *Nikora et al.* [2002] to a drag due to the biofilm mat as reported by *Labiod et al.* [2007].

[37] If k_s had remained constant at constant flow discharge, the acceleration of flow and upward displacement of the zero-velocity plane would have yielded an increase in the friction velocity u_*. Here, the decrease in k_s compensated for the flow acceleration, leading to the very weak changes in the turbulent shear stress and u_{rms} profiles, in contrast to the experiments by *Labiod et al.* [2007], and eventually leading to a small decrease in the friction velocity u_* (see Table 3).

[38] The effects of algal mats on the surface roughness were considered in this investigation to be somewhat similar to those of rigid roughness. However, the universality of the turbulence above complex surface roughness is a contentious issue in current research. For instance, for elastic rods representative of crop fields, it has been shown that frequency-locking processes can drive well-defined Kelvin-Helmoltz vortices [see *Py et al.*, 2006]. The same lock-in mechanisms have been demonstrated for compliant walls interacting with a turbulent boundary layer [*Xu et al.*, 2003]. Strong modifications by an epilithic biofilm were not reported in the very detailed study by *Nikora et al*. [2002], most likely because they used low biomass systems. The decrease in the value of D_u at day 61 in the present study could indeed indicate a modification of the nature of the turbulence by the development of a thick biofilm mat. However even this modification does not fundamentally eliminate the roughness length k_s as a turbulence descriptor, since a log law can still be found for the double-averaged streamwise velocity profiles. However, how the values found for k_s are related to the roughness geometry is clearly not trivial, since contributions from wakes behind hemispheres and bubbles (pressure drag) or viscous boundary layers along the filaments (viscous drag) appear in the double-averaged equations, and also decide the closure form for the Reynolds tensor (in terms of an equivalent mixing length for double-averaged quantities, the vertical profile of which, in the canopy, will also determine the value of k_s in the log law). Thus, k_s together with the friction velocity u_*, extracted from double-averaged measurements above the canopy, is still a descriptor of the turbulence behavior above this time-evolving complex roughness, but methods used to estimate u_* have to be chosen with care.

4.3. Model Testing and Evaluation

[39] To test and evaluate the influence of the different equations on the detachment term, values simulated with the numerical resolution of equation (1) for the three detachment equations (5), (6), and (7) were compared with the experimental data. First, in order to determine the empirical and numerical parameters of the simulation, we looked at the parameters that gave the best simulations of the changes in AFDM and Chl-*a* for each of the three equations for the detachment term. We then calculated the mean values for the three equations for the maximum specific growth $\mu_{\max}$ (d^{-1}), the inverse half-saturation constant k_{inv} (g^{-1} m^2), and the initial biomass B_{init}. The values retained for the final simulation and the comparisons are summarized in the captions of Figures 8 and 9. These values, which are dependent on the specific conditions of our experiment in terms of nutrient availability, light incidence, temperature, turbulence intensity, shear stress, and algal composition, cannot be generalized to other conditions of growth of epilithic biofilm. For the chronic detachment that is the focus of this study, epilithic biofilm does not have the same morphology and tolerance for shear stress, and the magnitude of shear stress which causes detachment of algae differs significantly between species, particularly taxa growing in different flow regimes [*Moulin et al.*, 2008a]. Nevertheless, the values of C_{det} found converged toward values calibrated in *Uehlinger et al.* [1996] for simulations of the dynamics of Chl-*a* (44×10^{-6} to 149×10^{-3} s m^{-3} d^{-1}) in a Swiss pre-alpine gravel bed river and those reported by *Boulêtreau et al.* [2006, 2008] for AFDM dynamics simulations (16×10^{-4} to 8×10^{-2} s m^{-3} d^{-1}) in the Garonne River. The values of C''_{det} were also within the range of values reported by *Fothi* [2003] (0–67×10^{-4} d^{-1} for simulations of the dynamics of AFDM and 7×10^{-4} to 4×10^{-3} d^{-1} for simulations of the dynamics of Chl-*a* in his experimental channel). For C'_{det} our values were completely outside the range values given in *Labiod et al.* [2007] in simulations of the dynamics of Chl-*a* (2×10^{-3} to 4×10^{-3} s m^{-1} d^{-1} in their experimental channel) and no values of the parameter C'_{det} associated with simulations of the dynamics of AFDM were found in the literature.

[40] As can be seen in Figure 8, simulation with a detachment function for the discharge Q as proposed by *Uehlinger et al.* [1996] overestimated the values measured in the phase of growth. While the simulated peak (30.9 g m^{-2}) calculated for day 43 was close to the measured value (32.8 ± 3.4 g m^{-2}) reached 44 days after inoculum, the loss in the detachment phase was not simulated by the model. Thus, with this equation, the values of AFDM stabilized at the peak reached. The value of the Nash-Sutcliffe coefficient of efficiency $E = 0.35$ indicates that this simulation is unsatisfactory

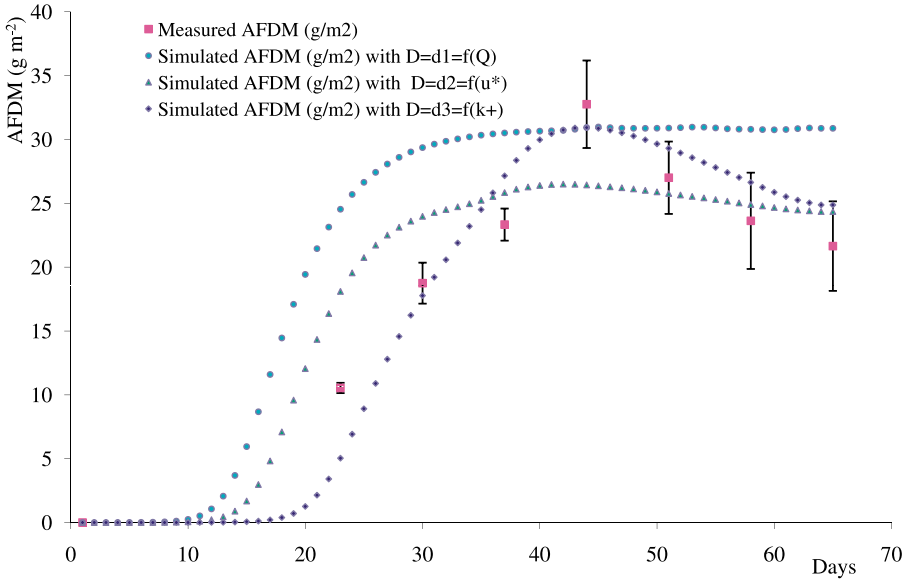

Figure 8. Comparison of measured AFDM (g m^{-2}) and simulated values with the three equations (5), (6), and (7) for detachment, *D:* $d_1 = C_{det} Q\, B$ ($\chi^2 = 1297$, $E = 0.35$), $d_2 = C'_{det} u_* B$ ($\chi^2 = 371$, $E = 0.82$), and $d_3 = C''_{det} k^+ B$ ($\chi^2 = 198$, $E = 0.91$); and with $B_{init} = 10^{-4}$ g m^{-2}, $\mu_{max} = 1.1$ d^{-1}, $k_{inv} = 0.085$ g^{-1} m^2, $C_{det} = 0.022$ s $m^{-3}d^{-1}$, $C'_{det} = 15$ s $m^{-1}d^{-1}$, and $C''_{det} = 0.0014$ d^{-1}.

($E < 0.36$). We must emphasize that in our case the discharge Q was kept constant, in contrast to the natural Swiss prealpine river and Garonne River flows for which this model was developed and tested by *Uehlinger et al.* [1996] and, more recently, by *Boulêtreau et al.* [2006]. The model reproduces catastrophic detachment driven by successive river floods.

[41] The values simulated with friction velocity u_* as an external variable of detachment gave a perfect estimation ($E = 0.82 > 0.75$) of the measured values at the growth and detachment phases, but the value of the simulated peak (26.5 for day 41 after inoculum) was far from the measured value. It can also be seen in Figure 8 that the third model,

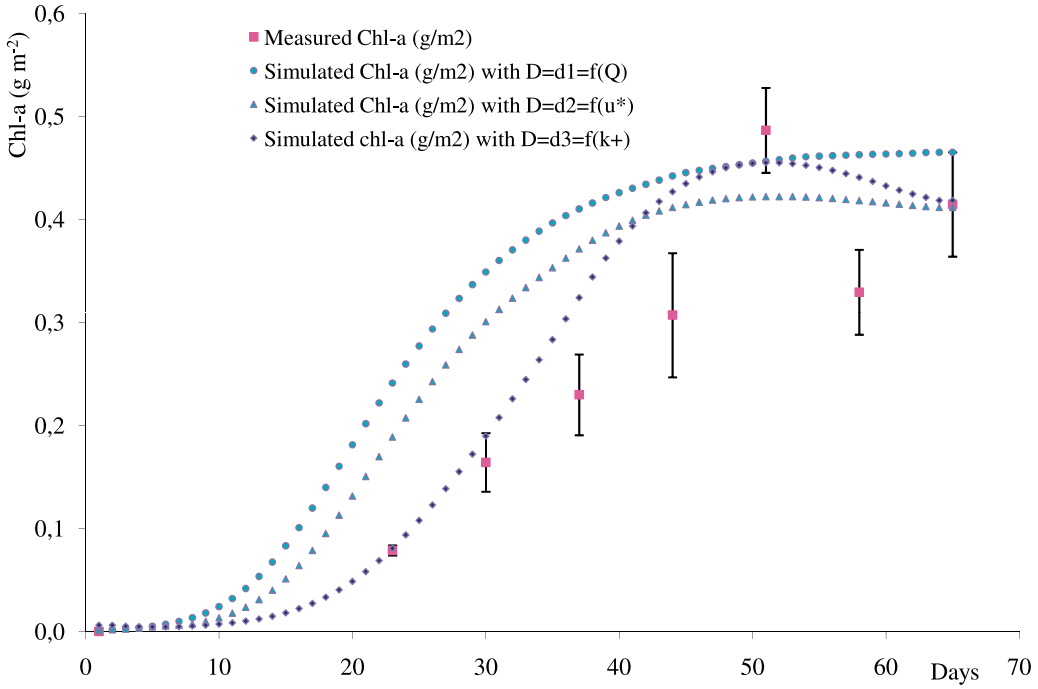

Figure 9. Comparison of measured Chl-*a* (g m^{-2}) and simulated values with the three equations (5), (6), and (7) for detachment, *D:* $d_1 = C_{det} Q\, B$ ($\chi^2 = 1182$, $E = 0.34$), $d_2 = C'_{det} u_* B$ ($\chi^2 = 555$, $E = 0.63$), and $d_3 = C''_{det} k^+ B$ ($\chi^2 = 18$, $E = 0.81$); and with $B_{init} = 10^{-3}$ g m^{-2}, $\mu_{max} = 0.5$ d^{-1}, $k_{inv} = 4.3$ g^{-1} m^2, $C_{det} = 0.0115$ s $m^{-3}d^{-1}$, $C'_{det} = 7.3$ s $m^{-1}d^{-1}$, and $C''_{det} = 0.00075$ d^{-1}.

with the roughness Reynolds number k^+ ($=u_* k_s/\nu$) as external variable of detachment, gave a more accurate simulation ($E = 0.91$) because the value of E is not only greater than 0.75, but also greater than the value found in the simulation with friction velocity u_* as an external variable of detachment. This is also confirmed by the decrease in the value of conformity χ^2 with $\chi^2 = 1297$ for $d1 = C_{\mathrm{det}} Q B$; $\chi^2 = 371$ for $d2 = C'_{\mathrm{det}} u_* B$; and $\chi^2 = 198$ for $d3 = C''_{\mathrm{det}} k^+ B$. The same tendencies can be observed in Figure 9, where the results of simulated changes in Chl-*a* (g m^{-2}) are plotted along with experimental data. Although the agreement was not as good as with AFDM, this could be because the AFDM biomass descriptor gives a balance sheet of the total organic production and mortality, whereas Chl-*a* only represents autotrophic production. The values of E and χ^2 found for the Chl-*a* simulations were $E = 0.34$ (unsatisfactory) and $\chi^2 = 1182$ for $d1 = C_{\mathrm{det}} Q B$; $E = 0.63$ (satisfactory) and $\chi^2 = 555$ for $d2 = C'_{\mathrm{det}} u_* B$; and $E = 0.81$ (perfect) and $\chi^2 = 18$ for $d3 = C''_{\mathrm{det}} k^+ B$.

[42] These results support the idea that transport phenomena that occur in the near-bed layer, such as chronic detachment of epilithic biofilm matter or vertical transport of nutrients and pollutants in submerged aquatic canopies [*Nepf et al.*, 2007], are not related to a single turbulence descriptor such as the friction velocity u_*, but require at least two descriptors, here the friction velocity u_* and the equivalent roughness height k_s. In our study of chronic detachment in the dynamics of epilithic matter, change in shear stress with the age of the epilithic biofilm is considered through a parameter that integrates the bottom roughness dimensions: The Nikuradse equivalent sand roughness k_s, which depends on the initial form and dimensions of the colonized substratum, and its changes owing to the thickness, resistance, and composition of the epilithic matter. This led us to conclude that the dynamics of epilithic matter can be better modeled and simulated by taking the roughness Reynolds number k^+ as the external variable of the detachment.

[43] In the literature, many different formulations have been proposed to model the detachment. Some authors use empirical expressions, *Horner et al.* [1983] propose the term $D = KV^{\theta}$, where V (cm s^{-1}) is the mean current velocity and could be easily replaced by the flow discharge Q, and θ is an empirical power law. Other authors use terms associated with some assumptions on the physics of the process, for example *Saravia et al.* [1998] propose the term $d_t B_t (V_t - V_m)^2$, where V_m (m s^{-1}) is the mean current velocity during biofilm growth, V_t (m s^{-1}) the actual current velocity, B_t (mg m^{-2}) the biomass, and d_t (s^2 m^{-2}) the degree of detachment produced by an increase in velocity (measured by $V_t - V_m$), with a square power law relating the detachment to an excess of kinetic energy. In the present study, we propose a term proportional to $k_s u_*$, a form that is closely related to simple parameterizations of the vertical mass flux Φ_v from the canopy layer to the external flow in turbulent boundary layers over roughness. For flows over urban canopies (e.g., winds over building-like roughness), *Bentham and Britter* [2003] and *Hamlyn and Britter* [2005] introduced the concept of exchange velocity U_E to describe this vertical mass flux as $\Phi_v = U_E(C_c - C_{\mathrm{ref}})$, where C_{ref} and C_c are the concentrations in the flow above and in the canopy, respectively. Those authors showed that U_E is proportional to the friction velocity u_*, with a factor that depends on the difference in velocity between the canopy layer and the flow above, that is, something indirectly related to the roughness length z_0 or, equivalently, to the roughness height k_s. If biofilm parts in direct contact with the flow and available for detachment (detached or dead parts) are now considered, their concentration in the canopy C_c will be proportional to the biomass quantity B, and far larger than the concentration in the flow above (i.e., $C_c - C_{\mathrm{ref}} \approx B$). Following *Bentham and Britter* [2003], the vertical flux of biomass from the canopy to the flow above would then read $\Phi_v = f(k_s) u_* B$, where $f(k_s)$ is a function of the roughness height k_s, in agreement with the detachment term proposed in the present study. In other words, the chronic detachment can be seen as a permanent extraction by the hydrodynamics of some part of the biomass that, together with the hemispheres, forms the canopy sublayer. This parameterization is supported by good agreement with the model developed by *Nepf et al.* [2007] for submerged aquatic canopies, where the vertical mass flux between the so-called exchange zone (upper part of the canopy) and the flow above reads $\Phi_v = k_e/\delta_e$, with $k_e = 0.19\, u_* (C_d a h)^{0.13}$ and $\delta_e = 0.23h/(C_d a h)$ obtained experimentally, yielding an expression reading $\Phi_v = 0.8 u_* (C_d a h)^{1.13}$, where C_d is the drag parameter for the plant rods and a their density. Since $C_d a h$ is proportional to k_s for sparse canopies, $0.8(C_d a h)^{1.13}$ can be seen as the function $f(k_s)$ discussed above. The equation proposed in the present paper, assuming proportionality with k_s, is then in relatively good agreement with the work of *Nepf et al.* [2007] and their 1.13 power law.

5. Conclusions

[44] In the present investigation, we tested the relevance of three formulations for chronic detachment of epilithic biofilm through numerical simulations with a simplified model adapted from *Uehlinger et al.* [1996]. In addition, we performed experimental studies in an indoor open channel flow to measure the growth of epilithic biofilm in interaction with turbulent rough flow and the evolution of local hydrodynamic parameters during epilithic biofilm growth.

[45] Laser Doppler anemometry measurements showed that the presence and growth of epilithic matter affected the hydrodynamic characteristics by acceleration of the mean flow and by changes in the turbulence intensity and shear stress, especially at the flow-biofilm interface. These changes were evaluated by estimation of the friction velocity, Nikuradse equivalent sand roughness, and dimensionless roughness Reynolds number, which gave net smoothing of the bottom roughness with the presence and growth of epilithic biofilm.

[46] Comparisons of the results of numerical simulations with biological measurements revealed that chronic detachment was better simulated by taking the roughness Reynolds number as the external variable of detachment. In fact, loss of epilithic matter was related not only to local hydrodynamic conditions, but also to changes in bottom roughness, which depended on the amount of the biofilm matter present and its form, and which was well described by the Nikuradse equivalent sand roughness k_s.

[47] It is important to underline that turbulence and shear stress not only control the detachment process, but also have a strong influence on the starting location of the colonization process around the substrate, as well as the transfer rates of nutrients, or carbon dioxide and oxygen, from the outer layer to inside the biofilm. Thus, the influence of turbulence and shear stress on the colonization and growth processes could be incorporated into future refinements of the model.

Notation

A log law roughness geometries constant.
AFDM ash free dry mass, g m^{-2}.
B biomass, g m^{-2}.
B_{init} initial biomass, g m^{-2}.
C colonization function, g m^{-2} d^{-1}.
C_{det}, C'_{det}, and C''_{det} empirical detachment coefficients, s m^{-3} d^{-1}, s m^{-1} d^{-1}, and d^{-1}, respectively.
Chl-*a* chlorophyll-*a*, g m^{-2}.
d displacement length, cm.
D detachment function, g m^{-2} $days^{-1}$.
G growth function, g m^{-2} $days^{-1}$.
k_{inv} inverse half-saturation constant, $g^{-1}m^{-2}$.
k_s Nikuradse equivalent sand roughness, cm.
k^+ roughness Reynolds number ($= u_* k_s/\nu$).
n number of acquisitions for a point of measurement by laser Doppler anemometry.
SE standard error in measured values, g m^{-2}.
U, V, W instantaneous velocity in the longitudinal, transversal, and vertical directions respectively, cm s^{-1}.
$\overline{U}$, $\overline{V}$, $\overline{W}$ time-averaged velocity in the longitudinal, transversal, and vertical directions, respectively, cm s^{-1}.
$\langle\overline{U}\rangle_{xy}$ double-averaged longitudinal velocity, cm s^{-1}.
u', w' root-mean-square value of longitudinal (u_{rms}) and vertical (w_{rms}) velocity, respectively, cm s^{-1}.
$\langle\overline{u'w'}\rangle_{xy}$ double-averaged turbulent shear stress, cm^2 s^{-2}.
u_* friction velocity, cm s^{-1} or m s^{-1}.
z distance from the flume bed, cm.
z_0 roughness length, cm.
μ_{max} maximum specific growth, d^{-1}.
N water kinetic viscosity, 10^{-6} m^2 s^{-1}.
Δ roughness height, cm.
K Von Karma universal constant ($\kappa \approx 0.4$).

[48] **Acknowledgments.** Myriam Graba was supported by the Algerian Ministry of the Higher Education and the Scientific Research in frame of the national program of training abroad (PNE). This work was supported by the national research project ACI-FNS (ECCO Ecosphère Continentale: Processus et Modélisation) and within the framework of the GIS-ECOBAG, Program P2 "Garonne Moyenne" supported by funds from CPER and FEDER (grant OPI2003-768) of the Midi-Pyrenees Region and Zone Atelier Adour Garonne) of PEVS/CNRS347 INSUE. We wish to thank A. Beer, S. Font, and G. Dhoyle for flume equipment and maintenance. We also thank anonymous reviewers for their critical comments.

References

Asaeda, T., and D. Hong Son (2000), Spatial structure and populations of a periphyton community: A model and verification, *Ecol. Modell.*, *133*, 195–207, doi:10.1016/S0304-3800(00)00293-3.

Asaeda, T., and D. Hong Son (2001), A model of the development of a periphyton community: Resource and flow dynamics, *Ecol. Modell.*, *137*, 61–75, doi:10.1016/S0304-3800(00)00432-4.

Auer, M. T., and R. P. Canale (1982), Ecological studies and mathematical modeling of *Cladophora* in Lake Huron: 3. The dependence of growth rates on internal phosphorus pool size, *J. Great Lakes Res.*, *8*, 93–99.

Belkhadir, R., B. Capdeville, and H. Roques (1988), Fundamental descriptive study and modelization of biological film growth: I. Fundamental descriptive study of biological film growth, *Water Res.*, *22*, 59–69.

Bentham, T., and R. Britter (2003), Spatially averaged flow over urban-like roughness, *Atmos. Environ.*, *37*, 115–125.

Biggs, B. J. F. (1996), Patterns in benthic algae of streams, in *Algal Ecology: Freshwater Benthic Ecosystems*, edited by R. J. Stevenson, M. L. Bothwell, and R. L. Lowe, pp. 31–56, Academic, San Diego, Calif.

Biggs, B. J. F., and C. W. Hickey (1994), Periphyton responses to a hydraulic gradient in a regulated river in New Zealand, *Freshwater Biol.*, *32*, 49–59.

Bothwell, M. L., D. Sherbot, A. C. Roberge, and R. J. Daley (1993), Influence of natural ultraviolet radiation on lotic periphytic diatom community growth, biomass accrual, and species composition: Short-term versus long-term effects, *J. Phycol.*, *29*, 24–35.

Boulêtreau, S., F. Garabetian, S. Sauvage, and J. M. Sánchez-Pérez (2006), Assessing the importance of self-generated detachment process in river biofilm models, *Freshwater Biol.*, *51*, 901–912, doi:10.1111/j.1365-2427.2006.01541.x.

Boulêtreau, S., O. Izagirre, F. Garabetian, S. Sauvage, A. Elosegi, and J. M. Sánchez-Pérez (2008), Identification of a minimal adequate model to describe the biomass dynamics of river epilithon, *River Res. Applic.*, *24*, 36–53, doi:10.1002/rra.1046.

Borchardt, M. A. (1996), Nutrients, in *Algal Ecology: Freshwater Benthic Ecosystems*, edited by R. J. Stevenson, M. L. Bothwell, and R. L. Lowe, pp. 183–227, Academic, San Diego, Calif.

Capdeville, B., R. Belkhadir, and H. Roques (1988), Fundamental descriptive study and modelization of biological film growth: I. A new concept of biological film growth modelization, *Water Res.*, *22*, 71–77.

Cheng, H., and I. P. Castro (2002), Near-wall flow over urban-like roughness, *Boundary Layer Meteorol.*, *104*, 229–259.

Flipo, N., S. Even, M. Poulin, M. H. Tusseau-Vuillemin, T. Ameziane, and A. Dauta (2004), Biogeochemical modeling at the river scale: Plankton and periphyton dynamics, Grand Morin case study, France, *Ecol. Modell.*, *176*, 333–347, doi:10.1016/j.ecolmodel.2004.01.012.

Fothi, A. (2003), Effets induits de la turbulence benthique sur les mécanismes de croissance du périphyton, Ph.D. dissertation, Inst. Natl. Polytech. de Toulouse, Toulouse, France.

Fuller, R. L., J. L. Roelofs, and T. J. Frys (1986), The importance of algae to stream invertebrates, *J. N. Am. Benthol. Soc.*, *5*, 290–296.

Ghosh, M., and J. P. Gaur (1998), Current velocity and the establishment of stream algal periphyton communities, *Aquat. Bot.*, *60*, 1–10.

Godillot, R., T. Ameziane, B. Caussade, and J. Capblanc (2001), Interplay between turbulence and periphyton in rough open-channel flow, *J. Hydraul. Res.*, *39*, 227–239.

Hamlyn, D., and R. Britter (2005), A numerical study of the flow field and exchange processes within a canopy of urban-like roughness, *Atmos. Environ.*, *39*, 3243–3254.

Hart, D., and C. M. Finelli (1999), Physical-biological coupling in streams: The pervasive effects of flow on benthic organisms, *Annu. Rev. Ecol. Syst.*, *30*, 363–395.

Hondzo, M., and H. Wang (2002), Effects of turbulence on growth and metabolism of periphyton in a laboratory flume, *Water Resour. Res.*, *38*(12), 1277, doi:10.1029/2002WR001409.

Horner, R. R., and E. B. Welch (1981), Stream periphyton development in relation to current velocity and nutrients, *Can. J. Fish. Aquat. Sci.*, *38*, 449–457.

Horner, R. R., E. B. Welch, and R. B. Veenstra (1983), Development of nuisance periphytic algae in laboratory streams in relation to enrichment and velocity, in *Periphyton of Freshwater Ecosystems*, pp. 121–164, edited by R. G. Wetzel, Dr. W. Junk, The Hague, Netherlands.

Jeffrey, S. W., R. F. C. Mantoura, and S. W. Wright (1997), *Phytoplankton Pigments in Oceanography*: *Guidelines to Modern Methods*, 661 pp., UNESCO, Paris.

Kliment, Z., J. Kadlec, and J. Langhhammer (2008), Evaluation of suspended load changes using AnnAGNPS and SWAT semi-empirical erosion models, *Catena*, *73*, 286–299, doi:10.1016:j.catena.2007.11.005.

Krause, P., D. P. Boyle, and F. Base (2005), Comparison of different efficiency criteria for hydrological model assessment, *Adv. Geosci.*, *5*, 89–97.

Labiod, C., R. Godillot, and B. Caussade (2007), The relationship between stream periphyton dynamics and near-bed turbulence in rough open-channel flow, *Ecol. Modell.*, *209*, 78–96, doi:10.1016/j.ecolmodel.2007.06.011.

Lekfir, A., T. A. Benkaci, and N. Dechemi (2006), Quantification du transport solide par la technique floue, application au barrage de Béni Amrane (Algérie), *Rev. Sci. Eau*, *19*, 247–257.

Lock, M. A., R. R. Wallace, J. W. Costerton, R. M. Ventullo, and S. E. Charlton (1984), River epilithon: Toward a structural-functional model, *Oikos*, *42*, 10–22.

Lopez, F., and M. Garcia (1998), Open-channel flow through simulated vegetation: Suspended sediment transport modeling, *Water Resour. Res.*, *34*, 2341–2352.

Lopez, F., and M. Garcia (2001), Mean flow and turbulence structure of open-channel flow through nonemergent vegetation, *J. Hydraul. Eng.*, *127*, 392–402.

Mayer, M. S., and G. E. Likens (1987), The importance of algae in a shaded headwater stream as a food of an abundant caddisfly (Trichoptera), *J. N. Am. Benthol. Soc.*, *6*, 262–269.

McIntire, C. (1973), Periphyton dynamics in laboratory streams: A simulation model and its implications, *Ecol. Monogr.*, *34*, 399–420.

McLean, S., and V. I. Nikora (2006), Characteristics of turbulent unidirectional flow over rough beds: Double-averaging perspective with particular focus on sand dunes and gravel bed, *Water Resour. Res.*, *42*, W10409, doi:10.1029/2005WR004708.

Mignot, E., E. Barthelemy, and D. Hurther (2009), Double-averaging analysis and local flow characterization of near-bed turbulence in gravel-bed channel flows, *J. Fluid Mech.*, *618*, 279–303, doi:10.1017/S0022112008004643.

Minshall, G. W. (1978), Autotrophy in stream ecosystems, *BioScience*, *28*, 767–771.

Momo, F. (1995), A new model for periphyton growth in running waters, *Hydrobiologia*, *299*, 215–218.

Moulin, F. Y., et al. (2008a), Experimental study of the interaction between a turbulent flow and a river biofilm growing on macrorugosities, in *Advances in Hydro-Science and Engineering*, vol. 8, edited by S. S. Y. Wang, pp. 1887–1896, Int. Assoc. Hydro-Environ. Eng. Res., Nagoya, Japan.

Moulin, F. Y., K. Mülleners, C. Bourg, and S. Cazin (2008b), Experimental study of the impact of biogenic macrorugosities on the benthic boundary layer, in *Advances in Hydro-Science and Engineering*, vol. 8, edited by S. S. Y. Wang, pp. 736–745, Int. Assoc. Hydro-Environ. Eng. Res., Nagoya, Japan.

Nepf, H., M. Ghisalberti, B. White, and E. Murphy (2007), Retention time and dispersion associated with submerged aquatic canopies, *Water Resour. Res.*, *43*, W04422, doi:10.1029/2006WR005362.

Nezu, I., and H. Nakagawa (1993), *Turbulence in Open-Channel Flows*, Balkema, Rotterdam, Netherlands.

Nielsen, T. S., W. H. Funk, H. L. Gibbons, and R. M. Duffner (1984), A comparison of periphyton growth on artificial and natural substrates in the upper Spokane River, *Northwest Sci.*, *58*, 243–248.

Nikora, V., D. Goring, and B. Biggs (1997), On stream periphyton-turbulence interactions, *N. Z. J. Mar. Freshwater Res.*, *31*, 435–448.

Nikora, V., D. Goring, and B. Biggs (1998), A simple model of stream periphyton-flow interactions, *Oikos*, *81*, 607–611.

Nikora, V., D. Goring, I. McEwan, and G. Griffiths (2001), Spatially averaged open-channel flow over rough bed, *J. Hydraul. Eng.*, *127*, 123–133.

Nikora, V., D. Goring, and B. Biggs (2002), Some observations of the effects of microorganisms growing on the bed of an open channel on the turbulence properties, *J. Fluid Mech.*, *450*, 317–341.

Nikora, V., I. McEwan, S. McLean, S. Coleman, D. Pokrajac, and R. Walters (2007a), Double averaging concept for rough-bed open-channel and overland flows: Theoretical background, *J. Hydraul. Eng.*, *133*, 873–883, doi:10.1061/(ASCE)0733-9429(2007)133:8(873).

Nikora, V., S. McLean, S. Coleman, D. Pokrajac, I. McEwan, L. Campbell, J. Aberle, D. Clunie, and K. Kol (2007b), Double-averaging concept for rough-bed open-channel and overland flows: Applications background, *J. Hydraul. Eng.*, *133*, 884–895, doi:10.1061/(ASCE)0733-9429(2007)133:8(884).

Py, C., E. de Langre, and B. Moulia (2006), A frequency lock-in mechanism in the interaction between wind and crop canopies, *J. Fluid Mech.*, *568*, 425–449, doi:10.1017/S0022112006002667.

Reiter, M. A. (1986), Interactions between the hydrodynamics of flowing water and development of a benthic algal community, *J. Freshwater Ecol.*, *3*, 511–517.

Reiter, M. A. (1989a), Development of benthic algal assemblages subjected to differing near-substrate hydrodynamic regimes, *Can. J. Fish. Aquat. Sci.*, *46*, 1375–1382.

Reiter, M. A. (1989b), The effect of a developing algal assemblage on the hydrodynamics near substrates of different size, *Arch. Hydrobiol.*, *115*, 221–244.

Saravia, L., F. Momo, and L. D. Boffi Lissin (1998), Modeling periphyton dynamics in running water, *Ecol. Modell.*, *114*, 35–47.

Stevenson, R. J. (1983), Effects of currents and conditions simulating autogenically changing microhabitats on benthic diatom immigration, *Ecology*, *64*, 1514–1524.

Stevenson, R. J. (1996), An introduction to algal ecology in freshwater benthic habitats, in *Algal Ecology*: *Freshwater Benthic Ecosystems*, edited by R. J. Stevenson, M. L. Bothwell, and R. L. Lowe, pp. 3–30, Academic, San Diego, Calif.

Uehlinger, U., H. Buhrer, and P. Reichert (1996), Periphyton dynamics in a flood prone pre-alpine river: Evaluation of significant processes by modeling, *Freshwater Biol.*, *36*, 249–263.

Wilcock, P. (1996), Estimating local bed shear stress from velocity observations, *Water Resour. Res.*, *32*, 3361–3366.

Winterbourn, M. J. (1990), Interactions among nutrients, algae, and invertebrates in a New Zealand mountain stream, *Freshwater Biol.*, *23*, 463–474.

Xu, S., D. Rempfer, and J. Lumley (2003), Turbulence over a compliant surface: Numerical simulation and analysis, *J. Fluid Mech.*, *478*, 11–34, doi:10.1017/S0022112002003324.

S. Boulêtreau, J. M. Sánchez-Pérez, and S. Sauvage, ECOLAB, Université de Toulouse, UPS, INPT, CNRS, Avenue de l'Agrobiopôle, BP 32607, Auzeville-Tolosane, Castanet-Tolosan, F-31326 Toulouse, France. (sabine.sauvage@ensat.fr)

O. Eiff and F. Y. Moulin, IMFT, Université de Toulouse, UPS, INPT, ENSEEIHT, CNRS, F-31400 Toulouse, France.

F. Garabétian, UMR 5805, Station Marine d'Arcachon, EPOC-OASU, Université Bordeaux 1, 2 Rue du Professeur Jolyet, F-33120 Arcachon CEDEX, France.

M. Graba and A. Kettab, Laboratoire des Sciences de l'Eau, Ecole Nationale Polytechnique, 10 Ave. Hassen Badi, El Harrach, Alger 16200, Algeria.